Lattice Polymers with Nearest-Neighbor Interactions: A Comparison of Polymer RISM Theory Employing Atomic Closures and Monte Carlo Simulations

R. H. C. Janssen, S. Wang, and E. Nies*

Department of Polymer Technology, Eindhoven University of Technology, P.O. Box 513, 5600 MB Eindhoven, The Netherlands

P. Cifra

Polymer Institute, Slovak Academy of Sciences, 842 36 Bratislava, Slovakia

Received November 3, 1997; Revised Manuscript Received April 23, 1998

ABSTRACT: A discretized version of the polymer RISM (PRISM) formalism using atomic closures has been applied to study the structural and thermal properties (the equation of state and liquid−gas spinodal) of the polymeric nearest-neighbor cubic lattice fluid. The obtained structural and equation of state properties are compared to *NpT* Monte Carlo simulations. From the comparison to the simulations, it follows that the predictions of the theory for both the structural correlations and the equation of state of the lattice fluid gradually worsen with increasing interaction strength. We find that the equation of state compares unfavorably with a, more conventional, nonrandom mixing-type theory based on the quasi-chemical approximation. We believe that the deterioration of the theory with increasing interaction strength is inherent in the PRISM plus atomic closure formalism and not typical for the lattice model studied in this work.

1. Introduction

This paper addresses the study of the thermal behavior of polymeric fluids (the equation of state and phase behavior). In principle, such behavior can be fully explained from the fluid's molecular organization. Since polymeric molecules generally consist of a linear sequence of covalently coupled particles (segments), we can attribute the molecular organization in a polymeric fluid to three types of interactions among the segments: covalent bonding and noncovalent attractive and repulsive interactions.

Classical theories for the thermal properties of polymers, such as cell,[1,2] lattice,[3−6] and hole theories,[7−9] do not derive thermal properties from a systematic calculation of this molecular organization. Instead, they introduce approximations at the level of the (canonical) partition function in order to obtain the thermal properties as accurately as possible.[10] Contrary, the more recently introduced polymer integral equation theories[11−14] do aim to calculate the fluid's molecular organization as precisely as possible, after which the equation of state (EoS) and phase behavior are obtained from the organization (quantified via segmental distribution functions) via well-established statistical mechanical routes.[15,16] Because of this clear link between the molecular and macroscopic material properties, integral equation theories provide insight that is much harder to obtain with the more conventional theories. This was our reason to compare the most successful polymer integral equation theory developed to date, namely the polymer RISM formalism,[11] to Monte Carlo simulation results, to test its numerical performance in predicting structural and thermal properties of polymer fluids. We have applied the theory to a particularly simple, but important, model: the polymeric cubic lattice fluid (for reasons explained below).

* To whom correspondence should be addressed.

It is well-known that the overall fluid structure, i.e., the sum of the inter- and intramolecular contributions, is largely determined by the repulsive interactions between the particle cores (packing effects) and that the effects of the attractive interactions and chain connectivity appear as perturbations on the structure caused by the particle cores.[17] Fortunately, it is possible to capture the packing effects within an integral equation approach to a high degree of accuracy, as is seen from our knowledge of the structural and equation of state properties of the hard-sphere model,[18−21] for which the repulsion between the particle cores is the sole factor that determines the fluid structure. Although of less importance for the overall fluid structure, it is nevertheless very desirable to incorporate also the effects of the attractive interactions and chain connectivity in a polymer theory, because of the decisive importance of these factors in describing phase behavior. Phase separation phenomena are very important in polymeric fluids and are believed to be dominated by a subtle balance of attractive interactions and chain connectivity effects,[22,23] although more recent work has shown that packing effects may also be a contributing factor in the phase separation of polymer fluids.[24−27]

The objective of the work presented here was to single out the influence of the attractive interactions and chain connectivity on the structural and thermal properties by removing the liquidlike ordering due to the repulsive particle cores (the packing effect). This is possible by discretizing the space available to the fluid on a cubic mesh, in other words, by studying cubic lattice fluids.[28] Previously, it was shown that such a discretization of space provides very clear-cut tests of the abilities of the Ornstein−Zernike integral equation[29] to account for the attractive interparticle interactions[30] and of the polymer RISM integral equation[11] to incorporate chain connectivity effects.[10] Here, we extend the work presented in a previous paper, ref 10, by incorporating attractive

10.1021/ma971611n CCC: $18.00
Published on Web 01/05/1999

interactions in the formalism. We calculate the structural correlations, the EoS, and the liquid−gas spinodal from a discretized version of the polymer RISM formalism. Thus far, we have not considered liquid−liquid miscibility behavior. It can certainly be studied within the PRISM formalism,[31,32] but here we consider the closely related[33] but simpler case of liquid−gas equilibrium first.

Apart from the possibility to study the performance of the polymer RISM equation without the predominant interference of liquidlike packing effects, the discretization of space allows comparison of the polymer RISM model with the vast body of existing polymer lattice results.[3−6] It is also less CPU-time-consuming to perform Monte Carlo simulations for lattice systems that are used for comparison with the polymer RISM results.

The contents of the rest of this paper are as follows. In section 2.1 we will briefly present the polymer RISM theory for lattice polymers subject to nearest-neighbor interactions. We have tested both the mean spherical approximation (MSA)[34] and Percus−Yevick (PY)[35] "atomic" closures. Thus far we have not studied the merits of the more recently introduced "molecular" counterparts of the MSA and PY closures.[36,37] Equations of state based on the energy MSA (e-MSA)[38] and the compressibility PY (c-PY)[39] route are given in section 2.2. Liquid−gas spinodal conditions are briefly recapitulated in section 2.3.[33,40] In section 3, the NpT MC simulations, from which the EoS and structural properties are extracted, are briefly outlined. Results are presented in section 4. The results for the intermolecular two-particle distribution of random flight 30-mers with segmental interaction energies of $u_{attr} = -0.05k_BT$ and $-0.2k_BT$ are calculated within the MSA and PY closure, and comparisons to MC simulations at varying packing fractions η_m are made. Results for the e-MSA and c-PY EoS are compared to NpT simulation results and to the EoS predicted by a nonrandom mixing lattice theory based on the quasi-chemical approximation.[6] Liquid−gas spinodals based on the c-MSA and c-PY route are calculated and compared to the LG spinodal obtained from the nonrandom mixing theory.[6] We also present RISM calculations obtained with a somewhat modified intramolecular distribution function and the intramolecular distribution function obtained from the MC simulations. Concluding remarks are presented in the final section 5.

2. Polymer RISM Theory

2.1. Structural Correlations on the Cubic Lattice. Consider a cubic lattice fluid consisting of flexible linear molecules that each consist of s covalently coupled segments. Segments occupy exactly one lattice site and are subject to the nearest-neighbor pair potential given by

$$\begin{aligned} u(0,0,0) &\to \infty \\ u(l,m,n) &= u_{attr} \quad \text{if } l^2 + m^2 + n^2 = 1 \\ u(l,m,n) &= 0 \quad \text{otherwise} \end{aligned} \tag{1}$$

where $(l,m,n) = \mathbf{r}_2 - \mathbf{r}_1$ with $\mathbf{r}_1$ and $\mathbf{r}_2$ being the positions of the two particles (segments) under consideration. The structural correlations in the nearest-neighbor polymeric lattice fluid can be characterized for long-chain molecules by two quantities:[11,41] a total intermolecular two-particle correlation, $h(l,m,n)$, and an intramolecular two-particle distribution, $\omega(l,m,n)$. The total intermolecular correlation can be expressed in terms of the intramolecular distribution function via the polymer RISM equation.[11] In Fourier space, it reads

$$\hat{h}(u,v,w) = \hat{\omega}(u,v,w)\,\hat{c}(u,v,w)(\hat{\omega}(u,v,w) + \eta_m\hat{h}(u,v,w)) \tag{2}$$

where η_m is the packing fraction of the segments. The Fourier transformation for symmetric functions $f(l,m,n) = f(\pm l,\pm m,\pm n)$ is defined on a cubic lattice by[28]

$$\hat{f}(u,v,w) = \sum_{l,m,n} f(l,m,n)\cos lu \cos mv \cos nw \tag{3}$$

The complementary real space quantity $f(l,m,n)$ is then obtained from $\hat{f}(u,v,w)$ by the inverse transformation

$$f(l,m,n) = \left(\frac{1}{2\pi}\right)^3 \int_{-\pi}^{\pi}\int_{-\pi}^{\pi}\int_{-\pi}^{\pi} \hat{f}(u,v,w) \times \cos lu \cos mv \cos nw \, du\, dv\, dw \tag{4}$$

Thus, $\hat{h}(u,v,w)$ and $\hat{\omega}(u,v,w)$ in eq 2 are respectively the Fourier transformed intermolecular correlation function and the intramolecular two-particle distribution. The $\hat{c}(u,v,w)$ is the Fourier transformed direct correlation function.

In a dense polymer melt, the spatial distribution of the segments of a polymer molecule can be given to a first approximation by a random flight (RF).[42] This corresponds to an $\hat{\omega}(u,v,w)$ given by[10,43]

$$\hat{\omega}_{RF}(u,v,w) = \frac{1 - \hat{\tau}^2 - (2/s)\hat{\tau} + (2/s)\hat{\tau}^{s+1}}{(1 - \hat{\tau})^2} \tag{5}$$

where $\hat{\tau}(u,v,w) = {}^1/_3(\cos u + \cos v + \cos w)$ is the one-jump probability.[43] In eq 5 it is implicit that the positions of the segments of a chain are only dependent on the position of the previous segment. Thus, the RF chain is not subject to excluded-volume interactions. The validity of eq 5 as a model for the intramolecular structure of linear chains has been confirmed experimentally for dense homopolymer melts,[44] but is doubted for polymer mixtures,[45] and can certainly not be used in polymer solutions.[46]

The total real space intermolecular two-particle correlation $h(l,m,n)$ is obtained from eq 2 by inverse transformation of $\hat{h}(u,v,w)$ according to eq 4

$$h(l,m,n) = \left(\frac{1}{2\pi}\right)^3 \int_{-\pi}^{\pi}\int_{-\pi}^{\pi}\int_{-\pi}^{\pi} \frac{\hat{\omega}^2(u,v,w)\,\hat{c}(u,v,w)}{1 - \eta_m\hat{\omega}(u,v,w)\,\hat{c}(u,v,w)} \times \cos lu \cos mv \cos nw \, du\, dv\, dw \tag{6}$$

It is seen from eq 6 that $h(l,m,n)$ can be obtained for a random flight chain fluid for known segmental packing fraction η_m and $\hat{c}(u,v,w)$. The real space direct correlation function, $c(l,m,n)$, from which $\hat{c}(u,v,w)$ can be constructed via eq 3, is given by a closure relation supplementing the discretized polymer RISM equation. Here, we study the MSA closure,[34] which for the nearest-neighbor model is given by

$$\begin{aligned} g(0,0,0) &= 0 \\ c(l,m,n) &= -\beta u_{attr} \quad \text{if } l^2 + m^2 + n^2 = 1 \\ c(l,m,n) &= 0 \quad \text{if } l^2 + m^2 + n^2 > 1 \end{aligned} \tag{7}$$

and the PY closure[35]

$$g(0,0,0) = 0$$
$$c(l,m,n) = g(l,m,n)(1 - e^{\beta u_{attr}}) \quad \text{if } l^2 + m^2 + n^2 = 1$$
$$c(l,m,n) = 0 \quad \text{if } l^2 + m^2 + n^2 > 1 \tag{8}$$

where the real space intermolecular two-particle distribution, $g(l,m,n)$, is related to the intermolecular two-particle correlation, $h(l,m,n)$, by

$$h(l,m,n) = g(l,m,n) - 1 \tag{9}$$

Note that the PY and MSA closures are identical for athermal systems ($u_{attr} = 0$). The nonoverlap condition in eqs 7 and 8, $g(0,0,0) = 0$, is physically exact and ensures that segments cannot occupy the same lattice site. The second condition in both closures, namely the contact relation, represents the effect of the attractive interactions on the correlations. The third relation, $c(l,m,n) = 0$, ensures that the direct correlation has the same reach as the segment−segment interactions. Note that the attractive interactions are incorporated directly into the RISM framework via the closure equations. Equations 5, 6, 7 or 8, and 9 form a complete set of equations from which the two-particle distributions of the nearest-neighbor RF polymer model can be obtained.

The set of equations is solved (see also ref 10) by constructing $\hat{c}(u,v,w)$ from the closure equation and eq 3. For the MSA closure we have $\hat{c}(u,v,w) = c_0 - 2\beta u_{attr}$-(cos u + cos v + cos w) with $c_0 = c(0,0,0)$. The unknown c_0 is then found by combining eq 6 with the nonoverlap condition and solving the resulting equation iteratively by a Newton−Raphson procedure combined with a 3D quadrature routine. Once c_0 is known, $g(l,m,n)$ is constructed from eqs 6 and 9.

For the PY closure, $\hat{c}(u,v,w) = c_0 + 2c_1$(cos u + cos v + cos w) with $c_0 = c(0,0,0)$ and $c_1 = c(\pm1,0,0) = c(0,\pm1,0) = c(0,0,\pm1)$. The unknowns c_0 and c_1 are found by combining eq 6 with the nonoverlap condition and the contact relation and solving the two resulting equations iteratively. The $g(l,m,n)$ is again obtained from eq 6 for known c_0 and c_1.

2.2. Equation of State. In this section we briefly recapitulate two ways of obtaining the equation of state of a polymeric lattice fluid. Both express the pressure in terms of a single thermodynamic state. They are the compressibility route, in the case where the PY closure is considered,[39] and the energy route when the MSA closure is considered.[38]

The general form of the pressure derived from the lattice compressibility EoS given by[10]

$$\frac{pv_0}{k_B T} = \int_0^{\eta_m} \left(\frac{1}{\hat{\omega}(0,0,0)} - \eta'_m \hat{c}(0,0,0) \right) d\eta'_m \tag{10}$$

Baxter has shown that it is possible to analytically integrate this equation if the PY closure is used to calculate the fluid structure. His expression, when applied to the nearest-neighbor polymer lattice fluid, is given by[10]

$$\frac{pv_0}{k_B T} = \frac{\eta_m}{s} + \frac{\eta_m^2}{2}\left(-2c(0,0,0) + 6c(1,0,0)\left(\frac{c(1,0,0)}{1 - e^{\beta u_{attr}}} - 2 \right) \right) + \left(\frac{1}{2\pi} \right)^3 \int_{-\pi}^{\pi}\int_{-\pi}^{\pi}\int_{-\pi}^{\pi} (\eta_m \hat{\omega}(u,v,w)\, \hat{c}(u,v,w) + \ln(1 - \eta_m \hat{\omega}(u,v,w)\, \hat{c}(u,v,w)))\, du\, dv\, dw \tag{11}$$

where v_0 is the volume of one lattice site. Equation 11 is more convenient than eq 10, because in the first equation the direct correlation $\hat{c}(0,0,0)$ has to be known for all fluid states with packing fractions between 0 and η_m, whereas in eq 11, $\hat{c}(0,0,0)$ only has to be known at a single packing fraction η_m.

Stell and Høye[38] have derived an analytical expression for the pressure $p = -(\partial E/\partial V)_{S,N}$ obtained from the energy equation for a monomeric fluid that is considered within the MSA equation. Their expression has been generalized to molecular fluids; see, e.g., ref 47. For the nearest-neighbor polymer fluid the resultant equation reads

$$\frac{pv_0}{k_B T \eta} - \frac{pv_0}{k_B T \eta}\Big|_0 = -{}^1/_2 s^2 \eta(\hat{c}(0,0,0) - \hat{c}_0(0,0,0)) + - \frac{s}{2(2\pi)^3}\int_{-\pi}^{\pi}\int_{-\pi}^{\pi}\int_{-\pi}^{\pi}\left(\frac{1}{\eta_m} \ln(1 - \eta_m \hat{\omega}(u,v,w)\, \hat{c}(u,v,w)) + \frac{\hat{\omega}(u,v,w)\, \hat{c}(u,v,w)}{1 - \eta_m \hat{\omega}(u,v,w)\, \hat{c}(u,v,w)} \right) du\, dv\, dw + \frac{s}{2(2\pi)^3}\int_{-\pi}^{\pi}\int_{-\pi}^{\pi}\int_{-\pi}^{\pi}\left(\frac{1}{\eta_m} \ln(1 - \eta_m \hat{\omega}(u,v,w)\, \hat{c}_0(u,v,w)) + \frac{\hat{\omega}(u,v,w)\, \hat{c}_0(u,v,w)}{1 - \eta_m \hat{\omega}(u,v,w)\, \hat{c}_0(u,v,w)} \right) du\, dv\, dw \tag{12}$$

In eq 12 $\eta = \eta_m/s$ is the density of chain molecules. Quantities that carry a subscript 0 are obtained from the athermal, i.e., nonattracting, random flight lattice fluid,[10] which serves as a reference fluid in eq 12.

In obtaining eqs 11 and 12, one assumes that the molecular conformations are not dependent on the thermodynamic state of the fluid, i.e., that $\hat{\omega}(u,v,w)$ is independent of η_m and T. Although this is not correct (lowering the density of the fluid will result in a crossover from random flight conformational statistics to self-avoiding flight statistics), it is precisely the assumption underlying the standard polymer RISM theory (see eq 5).[10,11,41] The different EoSs only produce equivalent answers when the structural correlations are known exactly. Generally, the results obtained from eqs 11 and 12 will be different due to the approximate nature of the polymer RISM equation, the closure equations, and the intramolecular distribution function. The size of this thermodynamic inconsistency can be judged from the results presented in section 4.

2.3. Liquid−Gas Spinodal. Polymeric fluids in principle exhibit a liquid−gas (LG) transition under the appropriate thermodynamic conditions, although in practice the conditions may not be attainable. In this work we nevertheless calculate the LG spinodal of a 30-mer, because we have a general interest in the accuracy of the thermodynamic properties that can be obtained from the polymer RISM framework and also because the liquid−gas phase behavior of a one-component fluid is of importance in understanding liquid/liquid miscibility phenomena in solutions and blends.[22,23,33] The LG

spinodal is defined by[1]

$$\left(\frac{\partial^2 A}{\partial V^2}\right)_{N,T} = -\left(\frac{\partial p}{\partial V}\right)_{N,T} = 0 \tag{13}$$

with A the free energy. It should not be confused with the binodal, which is the line that connects all thermodynamic equilibrium states. The spinodal is the line that separates the thermodynamic regions in which the fluid is metastable and unstable.[1] Although a fluid with conditions located in either the metastable or the unstable region will ultimately always phase separate, the distinction between the metastable and unstable region is not purely formal: the mechanisms of phase separation are different in both regions.

The spinodal and binodal share the critical point, which occurs at the maximum of both curves, i.e., at $(\partial^3 A/\partial V^3)_{N,T} = 0$.[1] The temperature T_c belonging to the critical point is the highest temperature for which a LG transition occurs.

From eq 13 and the thermodynamic definition of the isothermal compressibility, $\kappa_T = -1/V(\partial V/\partial p)_{N,T}$, we see that $\kappa_T \rightarrow \infty$ at the spinodal. Since the isothermal compressibility is defined in the RISM framework by[10]

$$k_B T \frac{\eta_m}{v_0}\kappa_T = \left(\frac{1}{\hat{\omega}(0,0,0)} - \eta_m \hat{c}(0,0,0)\right)^{-1} \tag{14}$$

the compressibility spinodal condition is given by

$$\frac{1}{\hat{\omega}(0,0,0)} - \eta_m \hat{c}(0,0,0) = 0 \tag{15}$$

Equation 15 is used in this work to obtain the spinodals of nearest-neighbor lattice polymers within the MSA and PY closures. Due to the approximate nature of the polymer RISM and closure equations, the MSA and PY spinodals will in general be different.

3. Monte Carlo Simulation

A previously employed NpT simulation method[6] was used for obtaining the inter- and intramolecular two-particle distributions and the EoS for interacting 30-mers with $u_{attr} = -0.05k_BT$ and $-0.2k_BT$ at varying packing fractions. The simulation details have been described elsewhere.[6,10] In the figures that follow, the error bars on the simulation results are smaller than the symbols in the figures and are therefore omitted. The CPU times needed to equilibrate a melt at a certain pressure were generally longer than for the athermal systems of ref 10. The longest runs for the highest densities ($\eta_m = 0.7$) took up to 30 h on a RISC IBM 6000 machine. The increase of CPU time, when compared to athermal systems, is mostly due to the higher packing fractions that interacting systems attain at comparable pressures.

4. Results and Discussion

4.1. Structural Correlations. In Figures 1-4 the two-particle distributions of interacting 30-mers are presented for $u_{attr} = -0.05k_BT$ at $\eta_m = 0.2885$ (Figure 1) and $\eta_m = 0.5301$ (Figure 2) and for $u_{attr} = -0.2k_BT$ at $\eta_m = 0.2940$ (Figure 3) and $\eta_m = 0.5681$ (Figure 4). Figures 1 and 3 depict the two-particle distribution belonging to a weakly and somewhat more strongly interacting fluid at a moderate density. Figures 2 and 4 depict the two-particle distributions of the same fluids

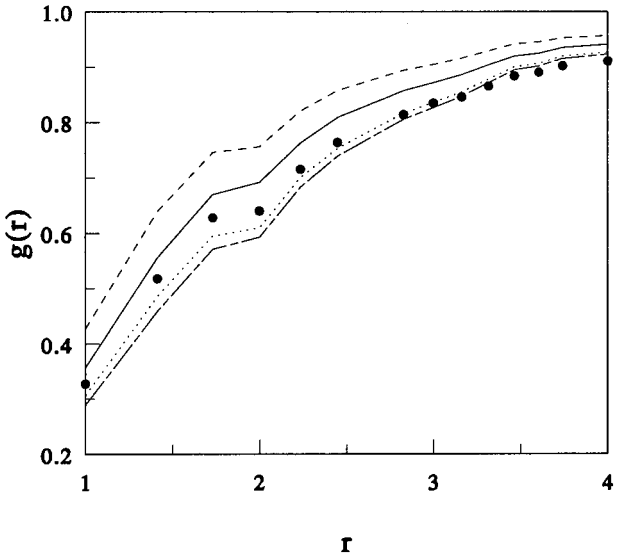

Figure 1. Intermolecular two-particle distribution of a 30-mer at $\eta_m = 0.2885$. The segmental interaction strength is $u_{attr} = -0.05k_BT$. The symbols represent results from MC simulation. The full and the dashed line denote the solution obtained with the PY and MSA closures, respectively, for the RF intramolecular distribution of eq 5. The long−short dash and dotted lines denote the respective results obtained with the PY and MSA closures for the corrected intramolecular distribution of eq 16.

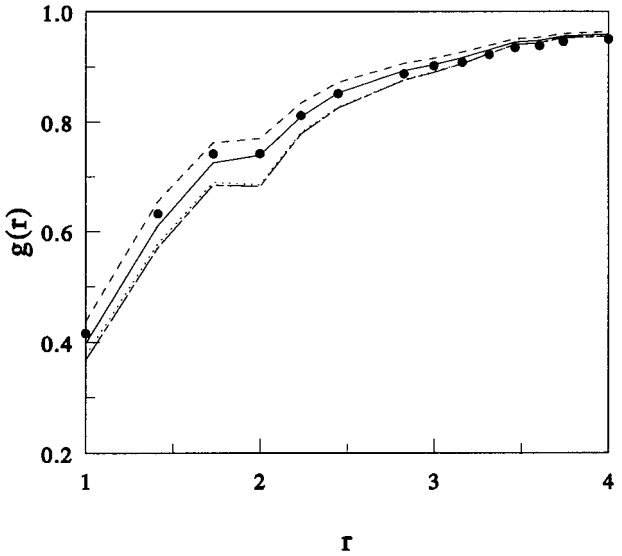

Figure 2. Intermolecular two-particle distribution of a 30-mer at $\eta_m = 0.5301$. Other details as in Figure 1.

at high density ($\eta_m > 0.5$ corresponds to fluids with chain properties of a dense polymer melt[48,49]). The intermolecular distribution, $g(l,m,n)$, obtained from the simulations is denoted by the symbols (●). The $g(l,m,n)$ obtained from the theory is indicated by the lines. All $g(l,m,n)$ are plotted as $g(r)$ with $r = \sqrt{l^2+m^2+n^2}$ for notational convenience.[10] It is noticeable from the nonmonotonic behavior of $g(r)$ that the cubic lattice fluid is slightly nonisotropic.[10] In Figures 1-4 the PY and MSA closures are denoted by the full and dashed line, respectively. The RF distribution given by eq 5 was used as an intramolecular distribution. Results obtained with a somewhat modified intramolecular distribution function, presented in eq 16, are also depicted by the dotted (MSA) and long−short dashed lines (PY). As a first approximation to improve upon the RF intramolecular

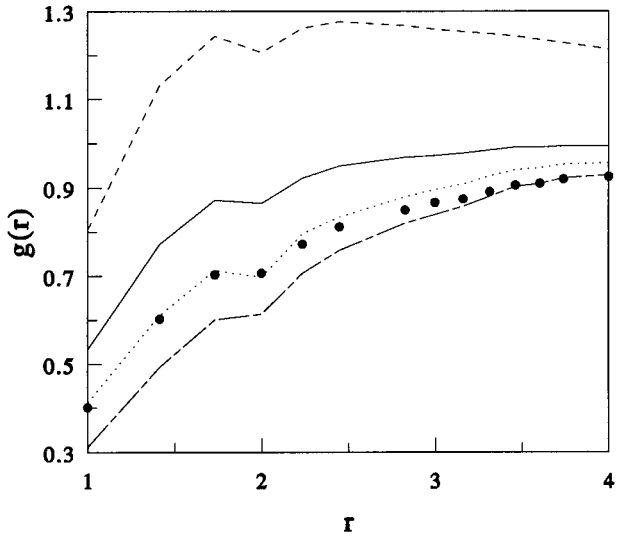

Figure 3. Intermolecular two-particle distribution of a 30-mer at $\eta_m = 0.2940$. The segmental interaction strength is $u_{attr} = -0.2k_BT$. Other details as in Figure 1.

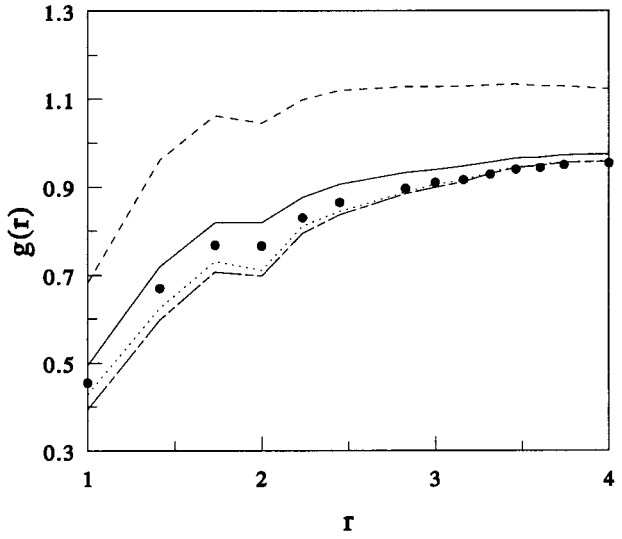

Figure 4. Intermolecular two-particle distribution of a 30-mer at $\eta_m = 0.5681$. The segmental interaction strength is $u_{attr} = -0.2k_BT$. Other details as in Figure 1.

distribution function, we have subjected $\hat{\omega}_{RF}(u,v,w)$ to a correction of its first few terms, viz.

$$\hat{\omega}_{corr}(u,v,w) = \hat{\omega}_{RF}(u,v,w) + (1 - \omega_{RF}(0,0,0)) + 2(\omega_{NRRW}(1,0,0) - \omega_{RF}(1,0,0))(\cos u + \cos v + \cos w) + 4(\omega_{NRRW}(1,1,0) - \omega_{RF}(1,1,0))(\cos u \cos v + \cos u \cos w + \cos v \cos w) \quad (16)$$

The term $(1 - \omega_{RF}(0,0,0))$ corrects for intramolecular particle overlaps inherent in the full RF intramolecular distribution $\hat{\omega}_{RF}(u,v,w)$. The other two terms have the effect that $\omega_{RF}(1,0,0)$ and $\omega_{RF}(1,1,0)$ are replaced by respectively $\omega_{NRRW}(1,0,0)$ and $\omega_{NRRW}(1,1,0)$, which are the values of the intramolecular distribution of a 3D Nonreversal Random Walk.[42] These values are more realistic than those given by $\omega_{RF}(1,0,0)$ and $\omega_{RF}(1,1,0)$ because unphysical back-folding of segment $i + 1$ on segment $i - 1$ is excluded in a NRRW chain and not in a RF chain. The values of the terms, given in Table 1, are obtained by enumeration of all possible chain conformations as is outlined in Appendix A of ref 10.

Table 1. Values of the Elements in the Terms of the Corrected Intramolecular Distribution Function of a 30-mer Given by Eq 16

$\omega_{RF}(0,0,0)$	1.618 743 160	$\omega_{NRRW}(1,0,0)$	0.476 023 356
$\omega_{RF}(1,0,0)$	0.645 332 143	$\omega_{NRRW}(1,1,0)$	0.239 736 684
$\omega_{RF}(1,1,0)$	0.305 167 785		

Note that $\hat{\omega}_{corr}(u,v,w)$ is not properly normalized, i.e., $\hat{\omega}_{corr}(0,0,0) \neq 30$. It would have been more correct to renormalize the long-range part of $\hat{\omega}_{corr}(0,0,0)$ such that $\hat{\omega}_{corr}(0,0,0) = 30$. We have not undertaken such a normalization, for in previous work it was shown that, in the case of athermal polymer chains, a complete absence of the tail contribution, i.e., $\omega(l,m,n) = 0$, for $r = \sqrt{l^2+m^2+n^2} > 4$, still produces accurate intermolecular distributions if the ω terms for $r \leq 4$ are accurate.[10] Thus, the minor changes in the tail values of $\omega(l,m,n)$ that will occur due to the normalization will not have a large influence on the results obtained with $\hat{\omega}_{corr}(u,v,w)$. Also, we have studied higher-order corrections than given in eq 16, but their influence on the structural and EoS properties was marginal, indicating that the lower-order terms of the intramolecular distribution function are indeed the most influential.

Figures 1−4 show that the intermolecular distributions predicted by the polymer RISM equation for the RF intramolecular distribution of eq 5 are not very accurate (full and dashed line) for both closures that were studied. In particular, in the fluid with stronger attractions between the segments it is seen that the calculated and simulated intermolecular distributions differ substantially (see Figures 3 and 4). For the weakly interacting systems, $u_{attr} = -0.05k_BT$, the difference between the simulations and calculations is smaller, although significant disparities are still observed at the lower density (see Figure 1). It is well-known (see, e.g., ref 46) that the average molecular configurations do not scale as random flights at low packing fractions. It is therefore not surprising that the largest disparities are observed at the lower packing fractions. Nevertheless, in ref 10 it is shown that RF chain statistics produces excellent structural results for athermal polymeric fluids considered at packing fractions as low as $\eta_m \approx 0.3$.

If the corrected intramolecular distribution is inserted in the polymer RISM equation, we see, by comparing the intermolecular distributions obtained with $\hat{\omega}_{RF}(u,v,w)$ and $\hat{\omega}_{corr}(u,v,w)$, that there is a very strong influence of the precise values of the first few terms in the intramolecular two-particle distribution on the intermolecular two-particle distribution, especially for $u_{attr} = -0.2k_BT$. In the case of the MSA closure, the use of $\hat{\omega}_{corr}(u,v,w)$ generally results in an improvement of the calculated intermolecular distribution function (compare dashed and dotted lines in Figures 1−4). In the case of the PY closure there generally is a shift from a too high to a too low contact value $g(1,0,0)$ upon changing from $\hat{\omega}_{RF}(u,v,w)$ to $\hat{\omega}_{corr}(u,v,w)$, and no real improvement is observed (compare full and long dash-short dashed lines in Figures 1−4).

Previously,[10] it was shown for athermal lattice fluids that the exact type of intramolecular distribution function used in the polymer RISM equation has little influence on the intermolecular distribution. The different intramolecular distributions that were studied all produced an accurate intermolecular distribution upon insertion in the polymer RISM equation, even at packing fractions as low as the ones considered in

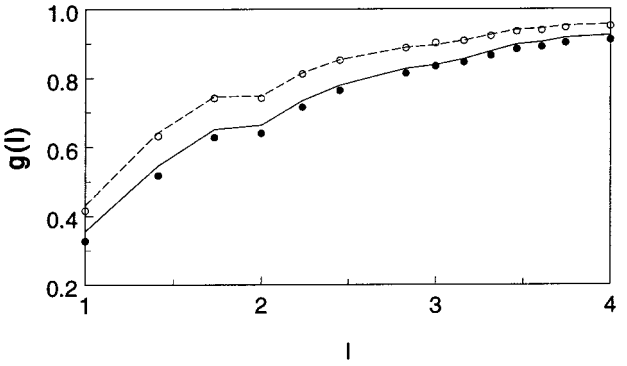

Figure 5. Intermolecular two-particle distribution of a 30-mer at $\eta_m = 0.5301$ (upper line) and $\eta_m = 0.2885$ (lower line). The segmental interaction strength is $u_{attr} = -0.05k_BT$. Symbols represent results from MC simulations. The lines are obtained by solving the polymer RISM plus PY equation with the intramolecular distribution obtained from MC simulation at the corresponding state point.

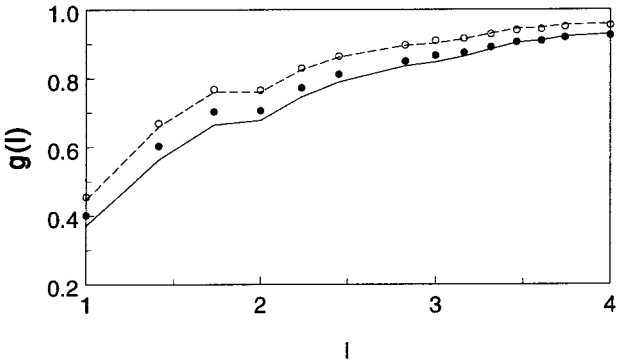

Figure 6. Intermolecular two-particle distribution of a 30-mer with $u_{attr} = -0.2k_BT$ at $\eta_m = 0.5681$ (upper line) and $\eta_m = 0.2940$ (lower line). Further legend as in Figure 5.

Figures 1 and 3. However, from Figures 1−4 it is seen that the intermolecular distribution shows an increased sensitivity for the exact values of the first few terms of the intramolecular distribution upon the introduction of attractive interactions: the sensitivity of $g(l,m,n)$ on $\omega(l,m,n)$ grows with increasing segmental interaction strength. We thus observe a gradual deterioration of the prediction for the intermolecular distribution with increasing segmental interaction strength using either $\hat{\omega}_{RF}(u,v,w)$ or $\hat{\omega}_{corr}(u,v,w)$. (Note that this is also the case in Figures 2 and 4 in which lattice fluids at densities for which RF statistics are known to be obeyed[48,49] are considered.) Clearly, for interacting systems, a simple RF model or the slightly more realistic form given in eq 16 is not sufficient for the PRISM equation when combined with the MSA or PY closure to produce accurate results. Therefore, in Figures 5 and 6 we have plotted the intermolecular two-particle distribution calculated from the PRISM equation and PY closure utilizing the exact intramolecular distribution obtained from MC simulations. (We only show results obtained with the PY closure since from Figures 1−4 it is seen that it performs better than the MSA closure.)

The intermolecular two-particle distributions depicted in Figures 5 and 6 are considered at the same state points as in Figures 1−4. It is seen from Figures 5 and 6 that the predicted intermolecular distribution functions are in close agreement with the pure MC results at the higher packing fractions (for which the correlations are less pronounced) but are further off for the moderate packing fractions (for which the correlations,

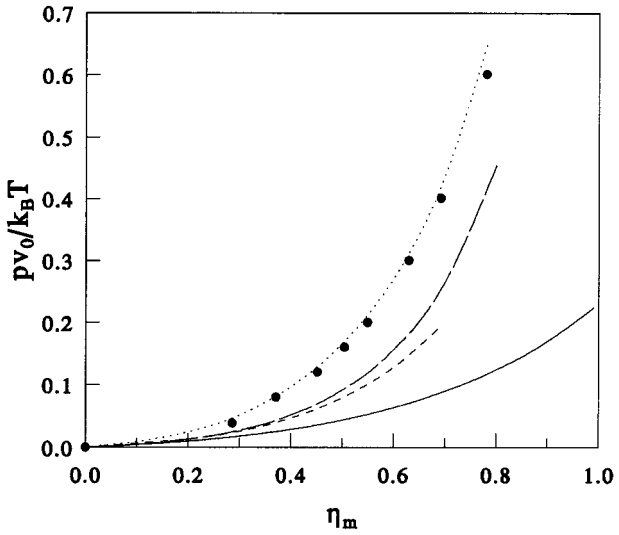

Figure 7. Equation of state of a 30-meric athermal cubic lattice fluid. The symbols are obtained from MC simulation, and the dotted line is obtained from eq 16 of ref 6. The full, short-dashed, and long-dashed lines are obtained from eq 11 for respectively the RF, NRRW, and corrected RF intramolecular distribution.

i.e., the deviations of $g(r)$ from 1, become more pronounced) despite the use of a very precise intramolecular distribution function. The above results lead us to conclude that the PRISM equation when combined with the PY or MSA closure is not able to accurately predict the intermolecular structural correlations in strongly correlated lattice fluids (i.e., strongly attracting fluids or fluids at moderate densities) even with a very accurate intramolecular distribution function as input. The above conclusion is not surprising since the RISM theory, on which the PRISM formalism is built, was originally devised to study the structure of weakly interacting systems.[50] Further, we believe that the reported failure cannot easily be cured. A solution to the problems, in our opinion, does not lie in constructing a self-consistent scheme,[51,52] since such a scheme does not alter the basic ingredients of the formalism: the polymer RISM and closure equations. A better option is offered in refs 36 and 37 in which the standard "atomic" MSA and PY closures are replaced by a more sophisticated ones. Thus far we have not investigated the quality of these "molecular" closures.

4.2. Equation of State. In Figures 7−9 the equations of state for 30-mers with segment−segment interactions of respectively $u_{attr} = -0.0k_BT$, $-0.05k_BT$, and $-0.2k_BT$ are shown. The symbols are obtained from NpT simulations. The dotted line in the figures is obtained from eq 16 of ref 6. It is a nonrandom mixing equation of state based on the quasi-chemical approximation.[53] It is seen from the figures that the NRM equation performs well in the three cases considered here. In Figures 7−9 we also display the EoS calculated with eqs 11 and 12, with $\hat{\omega}(u,v,w)$ taken either as a RF or from eq 16. (We have not inserted the intramolecular distributions obtained from the MC simulations in eqs 11 and 12, since the derivation of these equations assumes $\hat{\omega}(u,v,w)$ to be density-independent.)

For an athermal system the PY and MSA closures are identical, as are the EoS obtained via the c-PY and e-MSA route. In Figure 7 we therefore only consider c-PY results. The full and short dashed line in Figure 7 are reproduced, like the MC points, from previous

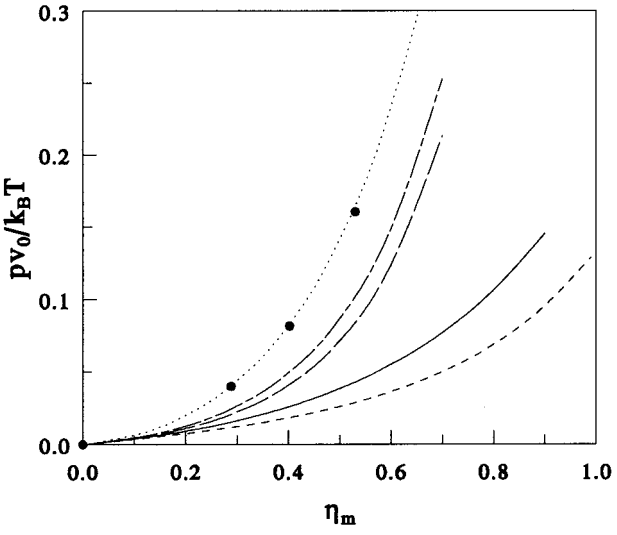

Figure 8. Equation of state of a 30-meric cubic lattice fluid with a segmental interaction energy $u_{attr} = -0.05k_BT$. The symbols are obtained from MC simulation, and the dotted line is according to eq 16 of ref 6. The full and long−short dashed lines are obtained from eq 11 (c-PY route) for the RF and corrected RF intramolecular distribution, respectively. The dashed and long dashed lines are obtained from eq 12 (e-MSA route), again for the RF and corrected RF distribution, respectively.

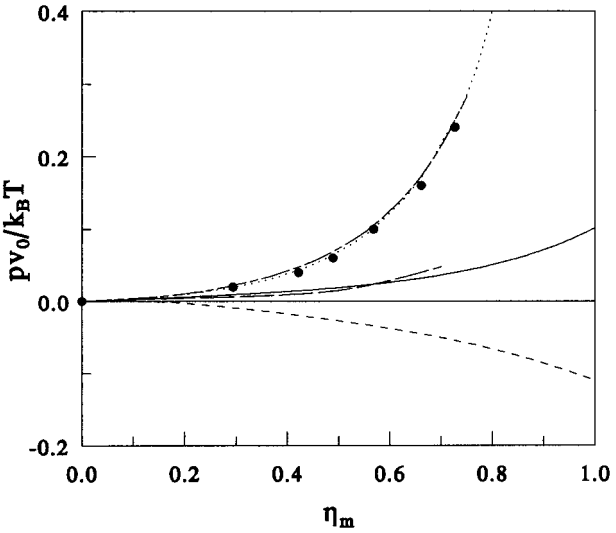

Figure 9. Equation of state of a 30-meric cubic lattice fluid with $u_{attr} = -0.2k_BT$. Legend as in Figure 8.

work[10] and show the EoS that are obtained for respectively the RF and NRRW intramolecular distribution. These EoS are reproduced in Figure 7, because we want to compare them to the EoS based on $\hat{\omega}_{corr}(u,v,w)$ of eq 16 (long dashed line). The NRRW intramolecular two-particle distribution produces an improved EoS, when compared to the RF intramolecular two-particle distribution, because, in contrast to the RF chain, excluded volume is partially taken into account in the NRRW chain. The $\hat{\omega}_{corr}(u,v,w)$ produces a more accurate EoS than the NRRW intramolecular distribution even though $\hat{\omega}_{corr}(u,v,w)$ is only different from the RF distribution in the first three terms (see eq 16). This is because in eq 16 we have set the first term of the corrected intramolecular distribution function to the physically correct value of $\omega_{corr}(0,0,0) = 1$, while $\omega_{NRRW}(0,0,0) > 1$. (A NRRW chain is subject to intramolecular particle overlaps.) This illustrates the importance of an accurate intramolecular distribution function for small segmental distances in predicting an EoS.

In Figure 8, the EoS of a weakly interacting ($u_{attr} = -0.05k_BT$) 30-mer is shown. The full and long−short dashed lines are obtained from the c-PY route (eq 11) for respectively the RF and corrected RF intramolecular distribution, and the dashed and long-dashed lines are obtained via the e-MSA route (eq 12), again for the RF and corrected RF distribution. As was the case for athermals, the use of the corrected intramolecular distribution function eq 16 results for both the c-PY and the e-MSA route in a significantly improved EoS.

The EoS for a more strongly interacting 30-mer fluid, $u_{attr} = -0.2k_BT$, is depicted in Figure 9. The different lines indicate the same comparative data as in Figure 8. The use of the corrected intramolecular distribution again leads to a large improvement in the EoS. However, comparing Figure 9 to Figures 7 and 8, we see that the overall consistency of the calculated EoS deteriorates with increasing segmental interaction strength, u_{attr}. We see that the sizes of the thermodynamic inconsistencies are huge for interacting polymer systems. It can also be observed in Figure 9, but equally so in Figures 7 and 8, that the calculated pressures do not rise to infinity at $\eta_m \rightarrow 1$. In all cases this is due to the (partial) neglect of chain excluded volume in $\hat{\omega}_{RF}(u,v,w)$ and $\hat{\omega}_{corr}(u,v,w)$.[10]

The observed inconsistencies between the EoS are a direct consequence of the failure of the PRISM equation when combined with the PY or MSA closure to produce accurate intermolecular particle distribution functions for polymeric fluids with attractive segmental interactions (see the previous section). We think that the observed inconsistencies for the EoS are inherently connected to the use of the polymer RISM framework and are model-independent. They also show up in continuum space models of attracting polymer fluids studied within the polymer RISM approach. A possible improvement may be offered by the molecular closures,[36,37] but so far we have not tested the merits of these closures.

4.3. Liquid−Gas Spinodal. In Figure 10 the compressibility MSA and c-PY liquid−gas spinodals are shown for 30-mers (section 2.3). Both curves were obtained with the RF chain distribution given by eq 5. Thus far, we have not calculated the spinodals with the corrected intramolecular distribution given by eq 16. Note that insertion of the RF intramolecular distribution in the spinodal condition eq 15 is more correct for the liquid branch of the spinodal than for the gaseous branch, because polymer chain conformations only scale like random flights in dense fluids.

The c-MSA and c-PY spinodals are compared to the LG spinodal calculated with the nonrandom mixing (NRM) theory of ref 6 and to the MC data of ref 54 for the binodal of 32-mer chains. Clearly, the NRM theory of ref 6 produces a critical point located at too weak an interaction strength. Such was also found in ref 55 for a NRM theory based on a slightly different model. The locations of the critical points produced by the c-PY and c-MSA routes are even further away from the MC data and are also located at interaction strengths that are too weak.

Apart from the locations of the c-PY (full curve) and c-MSA spinodal (dashed curve), these spinodals also display more severe anomalies. Both the c-PY and c-MSA spinodal cut $\eta_m = 1$ at finite u_{attr}, indicating that

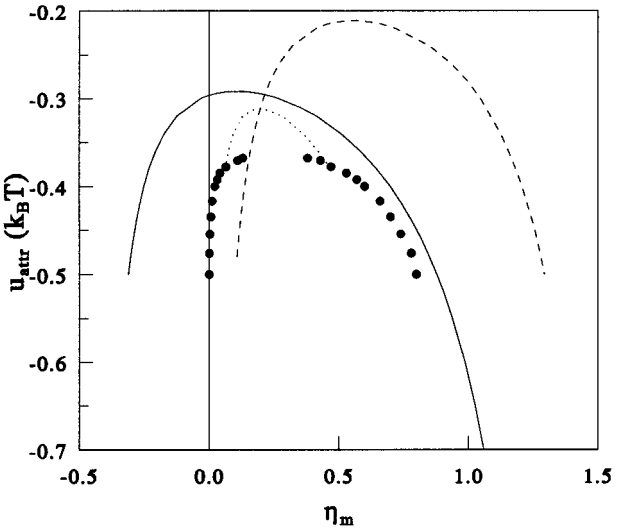

Figure 10. Liquid−gas spinodals for a cubic lattice fluid consisting of 30-mers. The dotted line is obtained from the nonrandom mixing theory of ref 6. The full and dashed lines are obtained for RF chains within the polymer RISM framework via the compressibility PY and compressibility MSA route, respectively. The symbols are MC data for the binodal of 32-mers taken from ref 54.

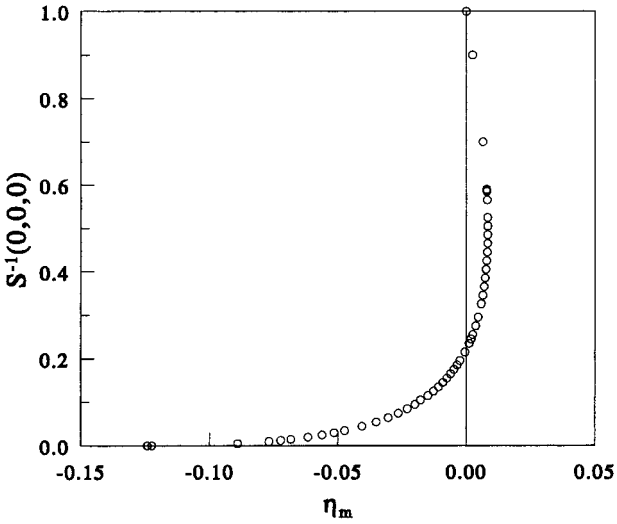

Figure 11. Dependence of the inverse structure factor at zero wave vector on η_m for a 30-mer lattice fluid at $u_{attr} = -0.32k_BT$. The $S^{-1}(0,0,0)$ is calculated within the PY closure.

there is a spinodal point at a finite segmental interaction strength on a fully packed lattice. This is clearly unphysical, since the isothermal compressibility should be zero for such an incompressible situation rather than infinite, which is the value needed to observe a spinodal point (see eqs 14 and 15). The anomaly is caused by the absence of excluded volume in the RF intramolecular distribution: due to the intramolecular segmental overlaps that are present if $\hat{\omega}_{RF}(u,v,w)$ is used, empty and doubly occupied sites occur at $\eta_m \rightarrow 1$, resulting in a nonzero compressibility. Improvements can certainly be expected for intramolecular two-particle distributions that do include the intramolecular excluded volume up to some extent.

The c-PY spinodal displays an additional anomaly: it also cuts $\eta_m = 0$ at finite segmental interaction strength. This is spurious, for the infinitely large distances between the molecules at $\eta_m \rightarrow 0$ prevent the molecules from interacting with each other, resulting in ideal gas behavior, for which a LG transition does not occur.

This anomaly is related to the use of the PY closure[56] and is not related to the use of a primitive intramolecular two-particle distribution, as is clear from the fact that the phenomenon is also observed in monatomic simple lattice[30] and continuum fluids.[57] Hence, the PY closure is fundamentally not suitable for investigating liquid−gas separation (and the closely related phenomenon of liquid−liquid phase separation[58]). The insuitability of the PY closure in calculating the LG spinodal via the compressibility route is illustrated in Figure 11, where the inverse structure factor at zero wave vector, defined by $S^{-1}(0,0,0) = (\sum_{l,m,n}\omega(l,m,n) + \eta_m h(l,m,n))^{-1}$, is plotted versus η_m at constant u_{attr}. As is seen from its definition and eqs 2 and 14, $S^{-1}(0,0,0) \sim \kappa_T^{-1}$: a spinodal point therefore corresponds to $S^{-1}(0,0,0) = 0$. The curve that can be drawn through the open circles in Figure 11 thus forms a trace of subsequent thermodynamic states, taken at fixed u_{attr}, with a decreasing value of $S^{-1}(0,0,0)$, that ultimately ends, as can be checked from Figure 10, on the gaseous branch of the spinodal when $S^{-1}(0,0,0) = 0$.

In Figure 11 it is seen that if $S^{-1}(0,0,0)$ is plotted versus packing fraction η_m at fixed u_{attr}, a nonfunctional form is obtained. (Note that we have partially plotted $S^{-1}(0,0,0)$ at negative η_m, which is necessary because the gaseous branch of the spinodal in Figure 10 cuts $\eta_m = 0$.) Thus, the result of Figure 11 contradicts thermodynamics, which states that the free energy, $A(\eta_m,u_{attr})$, and its derivatives with respect to η_m and u_{attr}, e.g., $S^{-1}(0,0,0)$, are state **functions**.[1] Hence, Figure 11 indicates that the gaseous branch of the LG spinodal obtained via the c-PY route has no physical meaning. If an $S^{-1}(0,0,0)$ trace that ends at the liquid branch is followed at $u_{attr} = \text{const}$, no anomalies are observed.

5. Conclusions

In this work we have discretized the PRISM equation to study a nearest-neighbor lattice fluid consisting of linear flexible polymeric molecules. We have used a random flight chain to generate the intramolecular two-particle distribution. The results for the intermolecular two-particle distribution, $g(l,m,n)$, obtained with the "atomic" PY and MSA closures, are shown to gradually deviate from NpT MC simulation results with increasing interparticle attraction. It was also shown that small changes in the values of the intramolecular distribution function at short interparticle distances have a tremendous effect on the intermolecular two-particle distribution. The effect increases with increasing $|u_{attr}|$. This sensitivity of $g(l,m,n)$ on $\omega(l,m,n)$ was not found for athermal lattice fluids[10] and requires the input of an $\omega(l,m,n)$ that is very accurate for small interparticle distances, although even for an exact $\omega(l,m,n)$ obtained from MC simulations, it is seen that the polymer RISM equation, when combined with the PY or MSA closure, is unable to provide an accurate description of the correlations in interacting polymer lattice fluids at lower densities.

Equations of state, calculated from the compressibility PY and energy MSA route, have also been presented. They are also shown to be very sensitive to the exact values of the first terms of $\omega(l,m,n)$. We again observe that the sensitivity increases with attractive interaction strength (which is not surprising: one obviously needs a good prediction for the fluid's structure to be able to accurately obtain its EoS).

Some results for the liquid−gas spinodal of 30-mer cubic lattice fluids are also presented. Although LG phase separation is not of vital importance in polymeric fluids, it is worthwhile to investigate, because of its close relation (see ref 33) with the very important liquid−liquid miscibility behavior of polymeric fluids. The spinodals that we have obtained were based on the compressibility PY and compressibility MSA route. The routes produce different spinodals, due to thermodynamic inconsistencies inherent in all integral equation approaches. The c-MSA and c-PY closures both show unphysical effects. In case of the c-MSA spinodal the anomalies are related to the absence of excluded volume in the intramolecular distribution. In case of the c-PY spinodal the anomalies are more fundamental and can be linked to of the closure itself.[30,57,58]

The polymer RISM theory, as used in the form presented here, is not able to properly account for the effects of attractive interactions between the molecule segments and produces an EoS that is markedly inferior to EoSs obtianed via conventional lattice techniques.[6] The strong dependence of the structural and thermodynamic properties on the intramolecular distribution function is a serious deficiency which we believe will be difficult to rectify. More accurate intramolecular distribution functions that might be obtained with help of MC simulations or a self-consistent scheme[51,52] are certainly important but do not cure the sensitivity of the polymer RISM theory on $\omega(l,m,n)$. Better options lie in altering the closure equations (see, e.g., refs 36 and 37 that employ a molecular closure) or the polymer RISM equation itself. So far we have not studied the merits of the molecular closures for cubic lattice fluids.

References and Notes

(1) Prigogine, I. *The Molecular Theory of Solutions*; North-Holland Publishing Company: Amsterdam, 1957.
(2) Flory, P. J.; Orwoll, R. A.; Vrij, A. *J. Am. Chem. Soc.* **1964**, *86*, 3567.
(3) Sanchez, I. C.; Lacombe, R. U. *J. Phys. Chem.* **1976**, *80*, 2352.
(4) Panayiotou, C.; Vera, J. H. *Fluid Phase Equilib.* **1980**, *5*, 55.
(5) Kleintjens, L. A.; Koningsveld, R. *Colloid Polym. Sci.* **1980**, *258*, 711.
(6) Nies, E.; Cifra, P. *Macromolecules* **1994**, *27*, 6033.
(7) Simha, R.; Somcynsky, T. *Macromolecules* **1969**, *2*, 341.
(8) Nies, E.; Xie, H. *Macromolecules* **1993**, *26*, 1683.
(9) Xie, H.; Nies, E. *Macromolecules* **1993**, *26*, 1689.
(10) Janssen, R. H. C.; Nies, E.; Cifra, P. *Macromolecules* **1997**, *30*, 6339.
(11) Curro, J. G.; Schweizer, K. S. *Macromolecules* **1987**, *20*, 1928.
(12) Chiew, Y. C. *Mol. Phys.* **1990**, *70*, 129.
(13) Wertheim, M. S. *J. Stat. Phys.* **1986**, *42*, 477.
(14) Yethiraj, A.; Hall, C. K. *J. Chem. Phys.* **1991**, *96*, 797.
(15) Hill, T. L. *Statistical Mechanics*; McGraw-Hill Book Company: New York, 1956; p 797.
(16) McQuarrie, D. A. *Statistical Mechanics*; Harper and Row Publishers: New York, 1976.
(17) Chandler, D.; Weeks, J. D.; Andersen, H. C. *Science* **1983**, *220*, 787.
(18) Wertheim, M. S. *Phys. Rev. Lett.* **1963**, *10*, 321.
(19) Martynov, G. A.; Sarkisov, G. N. *Phys. Rev. B* **1990**, *42*, 2504.
(20) Kincaid, J. M.; Weis, J. J. *Mol. Phys.* **1977**, *34*, 931.
(21) Carnahan, N. F.; Starling, K. E. *J. Chem. Phys.* **1969**, *51*, 635.
(22) Sanchez, I. C. *Annu. Rev. Mater. Sci.* **1983**, *13*, 387.
(23) Sanchez, I. C. In *Encyclopedia of Physical Science and Technology*; Academic Press: London, 1992; Vol. 11.
(24) Dijkstra, M.; Frenkel, D. *Phys. Rev. Lett.* **1993**, *72*, 298.
(25) Lekkerkerker, H. N. W.; Stroobants, A. *Physica A* **1993**, *195*, 387.
(26) Poon, W. C. K.; Warren, P. B. *Europhys. Lett.* **1994**, *28*, 513.
(27) Curro, J. G.; Schweizer, K. S. *Macromolecules* **1990**, *23*, 1402.
(28) Jancovici, B. *Physica* **1965**, *31*, 1017.
(29) Ornstein, L.; Zernike, F. *Proc. Kon. Ned. Acad. Wet.* **1914**, *17*, 793.
(30) Janssen, R. H. C. Structure and Thermodynamics of Lattice Polymers in Bulk and at Interfaces. Ph.D. Thesis, Eindhoven University of Technology, Eindhoven, The Netherlands, 1996; Chapter 2.
(31) Curro, J. G.; Schweizer, K. S. *Macromolecules* **1991**, *24*, 6736.
(32) Honeycutt, J. D. *Macromolecules* **1994**, *27*, 5377.
(33) Kirkwood, J. G.; Buff, F. P. *J. Chem. Phys.* **1951**, *19*, 774.
(34) Lebowitz, J. L.; Percus, J. K. *Phys. Rev.* **1966**, *144*, 251.
(35) Percus, J. K.; Yevick, G. J. *Phys. Rev.* **1958**, *110*, 1.
(36) Schweizer, K. S.; Yethiraj, A. *J. Chem. Phys.* **1993**, *98*, 9053.
(37) Yethiraj, A.; Schweizer, K. S. *J. Chem. Phys.* **1992**, *97*, 5927.
(38) Høye, J. S.; Stell, G. *J. Chem. Phys.* **1977**, *67*, 439.
(39) Baxter, R. J. *J. Chem. Phys.* **1967**, *47*, 4855.
(40) Schweizer, K. S.; Curro, J. G. *Macromolecules* **1988**, *21*, 3082.
(41) Curro, J. G.; Schweizer, K. S. *J. Chem. Phys.* **1987**, *87*, 1842.
(42) Flory, P. J. *Statistical Mechanics of Chain Molecules*; Hanser Publishers: Munich, 1989.
(43) Chandrasekhar, S. *Rev. Mod. Phys.* **1943**, *15*, 1.
(44) Lieser, G.; Fisher, E. W.; Ibel, K. *J. Polym. Sci., Polym. Lett. Ed.* **1975**, *13*, 39.
(45) Cifra, P.; Karasz, F. E.; MacKnight, W. J. *J. Polym. Sci., Polym. Phys. Ed.* **1988**, *26*, 2379.
(46) Freed, K. F. *Renormalization Group Theory of Macromolecules*; Wiley-Interscience: New York, 1987.
(47) Yethiraj, A.; Hall, C. K. *Mol. Phys.* **1991**, *72*, 619.
(48) Paul, W.; Binder, K.; Heermann, D. W.; Kremer, K. *J. Phys. II (France)* **1991**, *1*, 37.
(49) Müller, M.; Binder, K. *Comput. Phys. Commun.* **1994**, *84*, 173.
(50) Chandler, D. *Faraday Discuss. Chem. Soc.* **1978**, *66*, 71.
(51) Gyce, C. J.; Schweizer, K. S. *J. Chem. Phys.* **1994**, *100*, 6846.
(52) Gyce, C. J.; Yethiraj, A.; Schweizer, K. S. *J. Chem. Phys.* **1994**, *100*, 6857.
(53) Guggenheim, E. A. *Mixtures*; Oxford University Press: London, 1952.
(54) Yan, Q. L.; Liu, H. L.; Hu, Y. *Macromolecules* **1996**, *29*, 4066.
(55) Mackie, A. D.; Panagiotopoulos, A. Z.; Kumar, S. K. *J. Chem. Phys.* **1994**, *102*, 1014.
(56) Lomba, E. In *Supercritical Fluids*; Kiran, E., Levelt Sengers, J. M. H., Eds.; Kluwer Academic Publishers: Dordrecht, The Netherlands, 1994.
(57) Baxter, R. J. *J. Chem. Phys.* **1968**, *49*, 2770.
(58) Nies, E.; Wang, S.; Cifra, P.; Janssen, R. H. C., accepted.

MA971611N